Biochemistry

 Volume 37, Number 40 October 6, 1998

Articles

Crystal Structure and Possible Dimerization of the High-Potential Iron−Sulfur Protein from *Chromatium purpuratum*[†,‡]

Cheryl A. Kerfeld, Annette E. Salmeen,[§] and Todd O. Yeates*

Molecular Biology Institute, University of California at Los Angeles, 405 Hilgard Avenue, Los Angeles, California 90095-1570

Received May 4, 1998; Revised Manuscript Received August 10, 1998

ABSTRACT: The crystal structure of the high-potential iron−sulfur protein (HiPIP) isolated from *Chromatium purpuratum* is reported at 2.7 Å resolution. The three HiPIP molecules in the asymmetric unit of the crystals form one and one-half dimers. Two molecules are related by a noncrystallographic symmetry rotation of ∼175° with negligible translation along the dyad axis. The third molecule in the asymmetric unit also forms a dimer with a second HiPIP molecule across the crystallographic 2-fold symmetry axis. The Fe_4S_4 clusters in both the crystallographic and noncrystallographic dimers are separated by ∼13.0 Å. Solution studies give mixed results regarding the oligomeric state of the *C. purpuratum* HiPIP. A comparison with crystal structures of HiPIPs from other species shows that HiPIP tends to associate rather nonspecifically about a conserved, relatively hydrophobic surface patch to form dimers.

High-potential iron−sulfur proteins (HiPIPs)[1] are soluble proteins of 6−10 kDa in which a cubane Fe_4S_4 cluster is covalently linked to the polypeptide chain through four iron−cysteine bonds. HiPIPs are distinguished among the ferredoxins by their relatively high reduction potentials of +450 to +50 mV; the cluster charge changes from a +3 to a +2 state during reduction. In phototrophic eubacteria, they are found in the periplasmic space (*1*) functioning as a soluble electron carrier between the membrane-bound photoreaction center and the cytochrome bc_1 complex (*2*−*5*). Inactivation of the HiPIP gene in *Chromatium vinosum* is lethal (*6*), suggesting that HiPIP performs a critical cellular role. Additional functions have been proposed for HiPIP in the respiratory electron-transfer chain (*2*, *7*) and in sulfur oxidation (*1*, *8*). HiPIP has also been purified from two nonphototrophic species of bacteria. In a *Paracoccus* species (*9*), it is suggested to function as an electron donor to a nitrate reductase, and in *Thiobacillus ferrooxidans* (*10*), it is proposed to be a ferrous iron oxidase. The growing understanding of the versatility of Fe_4S_4 proteins for sensing oxygen or iron and in regulating transcription in other systems (summarized in ref *11*) may help illuminate the critical role of HiPIP.

Several lines of evidence suggest that HiPIP forms dimers that may be functionally relevant. In studies of self-exchange electron-transfer kinetics, most HiPIPs show very fast rates, indicative of a close association of HiPIP molecules in solution (*12*). EPR analysis of *C. vinosum* HiPIP suggests that the protein dimerizes (*13*). HiPIPs from several phototrophic species of bacteria have been crystallized and their

[†] This work was supported by the National Science Foundation's Postdoctoral Fellowship program in Plant Molecular Biology (C.A.K.) and USPHS GM 31299 (T.O.Y.).

[‡] The structural coordinates have been deposited in the Brookhaven Protein Data Bank under accession no. 3HIP.

* Corresponding author. E-mail: yeates@ewald.mbi.ucla.edu.

[§] Present address: Laboratory of Molecular Biophysics, Rex Richards Building, South Parks Road, Oxford, England OX13QU.

[1] Abbreviations: C, crystallographic symmetry; E_m, midpoint potential; EPR, electron paramagnetic resonance; HiPIP, high-potential iron−sulfur protein; NCS, noncrystallographic symmetry; pI, isoelectric point; rmsd, root-mean-square deviation.

S0006-2960(98)01025-3 CCC: $15.00
Published on Web 09/18/1998

three-dimensional structures determined. With the exception of *C. vinosum* HiPIP (*14*), the different HiPIPs pack within the crystal lattices as dimers (*15*−*17*). In each crystalline dimer, an approximate 2-fold axis of symmetry relates the molecules to allow close approach of the iron−sulfur clusters. Similar intercluster distances are observed in proteins that contain multiple, functionally linked iron−sulfur clusters. For example, the PsaC subunit of photosystem I contains two Fe_4S_4 clusters related by 2-fold rotational pseudosymmetry with an intercluster distance of 12 Å (*18*). Although the proteins did not pack as dimers in the *C. vinosum* HiPIP crystals, EPR data was used to model a dimerization interface (*19*) that is similar to those observed in other crystalline dimers. However, direct evidence for HiPIP dimerization in solution is scant. HiPIPs purified from most bacterial species behave as monomers in gel filtration columns, with the exception of that from *Rhodospirillum salinarum* (*20*) and *T. ferrooxidans* (*10*).

Here we report the crystal structure and the results of solution studies on the HiPIP isolated from *Chromatium purpuratum*. *C. purpuratum* is an anaerobic, marine species of purple-sulfur photosynthetic bacteria. As in other Chromatiaceae, the *C. purpuratum* reaction center contains a tetraheme cytochrome subunit that is presumably reduced by HiPIP. In the soluble fraction of *C. purpuratum*, HiPIP is the most abundant protein. It has significant N-terminal amino acid sequence homology to other HiPIPs isolated from *Chromatium* species and a relatively high midpoint potential of +390 mV (*21*). Under some conditions, *C. purpuratum* HiPIP appears to be a dimer in solution. Furthermore, the three molecules in the asymmetric unit of *C. purpuratum* HiPIP crystals are arranged as one and one-half dimers. A comparison of the crystallographic and noncrystallographic dimers to other crystalline HiPIP dimers is described in addition to the results of biochemical studies designed to detect the presence of HiPIP dimers in solution.

EXPERIMENTAL PROCEDURES

Biochemical Characterization. *C. purpuratum* HiPIP was purified by a combination of anion exchange and gel filtration chromatography as previously described (*21*). Analytical and preparative size-exclusion chromatography was carried out in a Toso Haas TSK3000 column (NOVEX Co., San Diego, CA) equilibrated in 25 mM sodium phosphate, pH 7.0/100 mM sodium sulfate, or in 300 mM sodium acetate, pH 5.5. The pH was adjusted with phosphoric acid, acetic acid, or sodium hydroxide, as appropriate. Alternatively, size-exclusion chromatography was carried out in a Superose 12 column (Pharmacia Corp. Uppsala, Sweden) equilibrated with 50 mM Tris, pH 8.0, 100 mM glycine, and 0.02% sodium azide. Elution was monitored at 280 nm. Gel filtration standards (1.35−670 kDa; Bio-Rad, Hercules, CA), cytochrome *c*-551, and horse heart cytochrome *c* (Sigma, St. Louis MO) were used for column calibration.

Dynamic light-scattering measurements were made with a Dyna-Pro-801 (Protein Solutions, Charlottesville, VA) of HiPIP at 1−4 mg/mL under several different buffer conditions: 50 mM Tris, pH 8.0, or 50 mM sodium phosphate, pH 5.5; for some measurements, a few grains of ferricyanide or 0.5 mM of buffered ascorbate was added prior to sampling. The data were analyzed with the Dyna-Pro software; for estimates of molecular weight for monodisperse samples, data points with baseline values between 0.995 and 1.005 were accepted.

Table 1: Data Collection and Refinement Statistics

refinement res limit (Å)[a]	8−2.8
$\langle I/\sigma \rangle$[b] (Overall/Last Shell)	6.9/3.3
completeness (%)	98.5
reflections	
unique	6568
total obs	13 850
working set	5767
test set	700
R-merge[c] (%)	12.2
R-factor[d] (%)	22.4
R-free (%)	28.8
no. of protein atoms	1839
average *B*-factor (Å^2) (main/side chain)	14.7/22.4
weighted rms deviations from ideality	
bond lengths (Å)	0.007
bond angle (deg)	1.3

[a] Using all data (no $\langle I/\sigma \rangle$ cutoff). [b] $\langle I/\sigma \rangle$ is the average ratio of the observed intensity to the estimated standard deviation. [c] *R*-merge = $100(\sum_i |I_i - \langle I \rangle| / \sum_i I_i)$, where the sum is taken over the unique reflections and $\langle I \rangle$ is the mean value of the multiple measurements of the ith intensity. [d] *R*-factor = $100(\sum |F_o - F_c| / \sum |F_o|)$.

Sedimentation equilibrium runs were performed on a Beckman Optima XL-A analytical ultracentrifuge using absorption optics. Solute concentrations were monitored at wavelengths of 280, 395, or 410 nm. A high band-pass filter was used for samples monitored at 410 nm. Sample concentration varied from 0.09 to 2.5 mg/mL. Samples were examined in six-channel 12 mm path length cells, double sector 12 mm path length cells, and at high concentrations, double sector 3 mm path length cells. Parallel experiments were run at either 4 or 20 °C in several different buffering conditions: (1) 10 mM Tris, pH 7.5, 100 mM sodium chloride; (2) 10 mM sodium acetate, pH 5.0, 0.15, or 1.0 M sodium chloride; (3) the FPLC size-exclusion chromatography mobile phase (50 mM Tris, pH 8.0, 100 mM glycine, and 0.02% sodium azide); and (4) HPLC size-exclusion chromatography mobile phase (25 mM sodium phosphate, pH 7.0, 100 mM sodium sulfate, and 0.02% sodium azide). Sedimentation profiles were measured at speeds of 15 000, 22 000, 24 000, or 28 000 rpm. The data were fitted with a nonlinear least-squares exponential fit for a single ideal species. A partial specific volume of 0.715 cm^3/g was estimated from the amino acid composition and the iron−sulfur cluster.

Crystallization and Structure Determination. Crystals of *C. purpuratum* HiPIP were readily obtained by vapor diffusion. The hanging drops contained 2 μL of 8.0 mg/mL protein in 5 mM Tris, pH 8.0, plus 2 μL of a reservoir solution containing approximately 3 M ammonium sulfate in the pH range 4.5−8.0. Crystal morphology varied between clusters of thin rods and thin lozenge-shaped plates. Crystals grown over a reservoir containing 3.2 M ammonium sulfate in 100 mM citrate, pH 5.4, were the bulkiest in all dimensions (~300 × 150 × 30 um) and were used for structure determination (Table 1). Diffraction data were collected on a RAXIS-II image plate detector with a Rigaku RU-300 X-ray generator. Diffraction data were processed using DENZO and SCALEPACK (*22*). The crystal lattice is primitive orthorhombic with cell dimensions of $a = 55.5$, $b = 108.8$, and $c = 37.2$ Å. An examination of the axial

Table 2: Primary Structures of High-Potential Iron−Sulfur Proteins[a]

E. halophila I	........EP	RAEDGHAHD**Y**	VNEAADASGH	PRYQ.....E	GQL**C**EN**C**AFW
C.gracile	.EVPANAVTE	SDPTAVALK**Y**	HRNAEASERV	AAARPGLPPE	EQH**C**EN**C**QFM
C. purpuratum	..VPANAVTE	SDPAAVALK**Y**	HRDAAESSRV	AAARPGLPPE	EQH**C**EN**C**QFM
C. vinosum	.SAPANAVAA	DNATAIALK**Y**	NQDATKSERV	AAARPGLPPE	EQH**C**AN**C**QFM
E. vacuolata II	....MERLSE	DDPAAQALE**Y**	RHDAS.SVQH	PAYE.....E	GQT**C**LN**C**LLY
Rc. tenuis (2761)	........GT	NAAMRKAFN**Y**	QDTAKN.....	....	GKK**C**SG**C**AQF

	51			87
E. halophila I	GEAVQ...DG	WGR**C**THPDF	DEVLVKAE**G**W**C**S	VYAPAS
C.gracile	LPDQGA..DE	WRG**C**SLFPG	..KLINLD**G**W**C**A	SWTLRAG
C. purpuratum	NPDQAA..AD	WKG**C**QLFPG	..KLINLS**G**W**C**A	SWTLRAG
C. vinosum	QADAAGATDE	WKG**C**QLFPG	..KLINVD**G**W**C**A	SWTLKAG
E. vacuolata II	TDASA...QD	WGP**C**SVFPG	..KLVSAN**G**W**C**T	AWVAR..
Rc. tenuis (2761)	VFGASPTAAG	..G**C**KVIPG	.DNQIAPG**G**Y**C**D	AFIVKK.

[a] The tentative primary structure of *C. purpuratum* HiPIP was assigned from the crystal structure (this work). Other primary structures are from the compilation of Van Driessche et al. (*31*). HiPIP structures characterized by X-ray crystallography are underlined. Conserved residues are in bold-faced type. Residues in the dimerization interface (making intermolecular contacts less than 4.5 Å) are double-underlined.

reflections suggested the space group $P2_12_12$. Data from two crystals were processed and merged to obtain a 98% complete data set to 2.8 Å resolution. Molecular replacement using the program AMORE (*23*) was successful using *C. vinosum* HiPIP as a search model. The search model included the metal cluster and the protein chain truncated to polyalanine with the exception of the four cysteinyl ligands and invariant Tyr 19. The *n*-body translation function was carried out in parallel in the $P2_12_12_1$ and the $P2_12_12$ space groups. The correlation coefficient and *R*-factor after positioning two of the molecules in the asymmetric unit confirmed the space group $P2_12_12$. The *R*-factor after positioning three molecules in the asymmetric unit in $P2_12_12$ was 47.7%. One cycle of positional refinement using XPLOR (*24*) decreased the *R*-factor to 41.9%. A phased anomalous difference Fourier was calculated from phases derived from the three molecules in the asymmetric unit after removal of the Fe_4S_4 clusters and all atoms within a 3.0 Å radius of the clusters. Electron density for the Fe_4S_4 clusters was observable to the 5.0σ contour level (data not shown), confirming the structure solution.

Completion of the amino acid sequence and manual model building was carried out using 3-fold real-space averaged electron density maps generated by RAVE (*25*), using all diffraction data. Electron density maps were visualized with FRODO (*26*) on an Evans and Sutherland computer graphics system. For refinement of the model, 10% of the data was withheld as a test set for calculation of *R*-free. Positional refinement of the model was carried out in XPLOR (*24*) using the Engh and Huber stereochemistry parameters (*27*) with the XPLOR metal cluster parameters appended. Strict noncrystallographic symmetry constraints were imposed throughout refinement of the model. Side-chain and main-chain grouped atomic displacement refinement was carried out during the final two refinement cycles.

Structure Analysis and Comparison. Protein superpositions were carried out using the program ALIGN (*28*). To position the other eubacterial HiPIP dimers in the same frame of reference as either the *C. purpuratum* noncrystallographic or crystallographic dimer, one molecule of the *C. purpuratum* dimer was chosen as reference molecule ("A"), the second as reference molecule "B". Then one molecule of each of the *Ectothiorhodspira halophila*, *Rhodocyclus tenuis*, and *Ectothiorhodospira vacuolata* HiPIP dimers was rotated onto A using ALIGN. The resulting rotation matrix and translation vector were used to map the second molecule of the *E. halophila*, *Rc. tenuis*, and *E. vacuolata* dimers into the *C. purpuratum* dimer reference frame. The relative disposition of this second molecule with respect to *C. purpuratum* molecule B was then calculated by ALIGN. In a similar manner, the *E. vacuolata* and *Rc. tenuis* dimers were compared to each other.

Values for solvent-exposed surface area were calculated using SURFACE (*29*) as implemented in the CCP4 programming package. The change in solvent-accessible surface area due to the putative oligomerization was calculated as half the difference between twice the surface area of the monomer and the surface area of the dimer.

RESULTS AND DISCUSSION

The Primary Structure of C. purpuratum HiPIP. With the exception of residues 10−13 and 52−57, real-space averaged electron density maps for the crystallographically constrained HiPIP molecule were of very good quality and permitted sequencing of most of the primary structure. Previously, the N-terminal amino acid sequence was determined by automated Edman degradation on dissolved crystals (*21*). The partial primary structure of *C. purpuratum* HiPIP was most similar to that of *Chromatium gracile* (Table 2) and *Chromatium tepidum*. In building into the electron

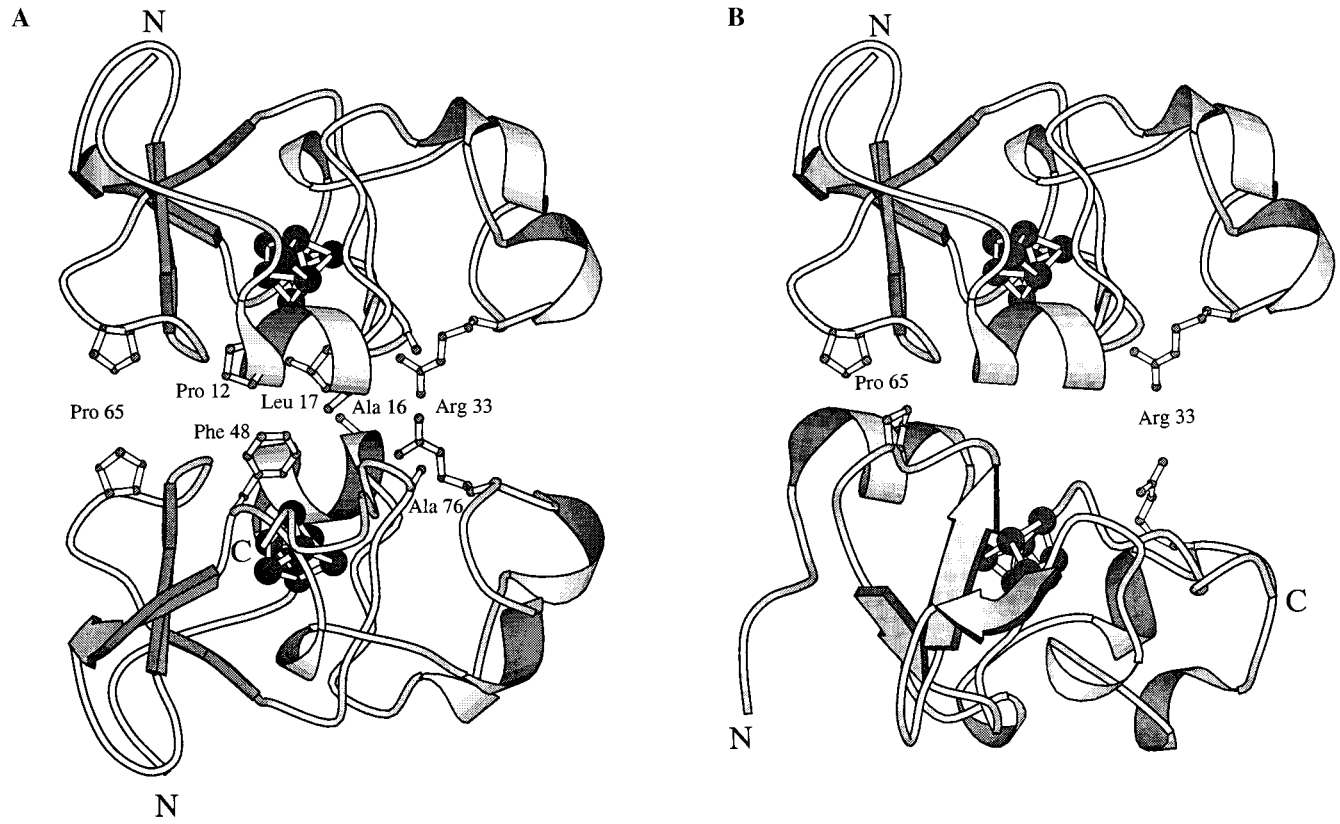

FIGURE 1: (A) The *C. purpuratum* dimers formed by noncrystallographic symmetry (NCS). The N- and C-termini are labeled. Atoms of the iron−sulfur cluster are shown in gray. Residues in the putative dimerization interface are shown in ball-and-stick representation and are labeled. (B) The dimer formed by the crystallographic 2-fold symmetry axis. The top molecule is positioned as in the NCS-dimer. Figure prepared using MOLSCRIPT (*43*).

density, this homology and the potential for hydrogen-bonding interactions were used for choosing between the carboxylic acid side chains (Asp and Glu) or their amide forms. Similar criteria were used for distinguishing Thr and Val.

The molecular mass of the model is 9187 Da, in fair agreement with the mass determined by ion spray mass spectrometry of dissolved crystals (9372 Da) and with the amino acid composition (data not shown). Some of the shortfall in molecular mass is likely due to missing acidic amino acids. Because of poor electron density, the N-terminal Glu residue was not built. Amino acid composition indicates that there should be 10 residues of the type Asx (Asp or Asn) and 12 Glx (Glu or Gln) residues as compared to 8 and 10 in the model, respectively. Moreover, the experimentally determined isoelectric point is lower [∼4.3 (*21*)] than the pI calculated from the model (5.3). Within the N-terminal sequence assigned by Edman degradation, electron density was not visible for side chains of Asp 10 and Thr 13. This is likely due to motion of the side chains since these residues are solvent exposed and not involved in intermolecular contacts. Three other side chains (Glu 27, Gln 53, and Gln 62) should be treated as tentative assignments due to their relatively high *B*-factors, despite the presence of electron density in omit maps.

Tertiary Structure. Similar to other HiPIP structures, *C. purpuratum* HiPIP consists of short regions of β-strand and α-helical secondary structure punctuated by turns and extended coils that shield the Fe_4S_4 cluster from solvent (Figure 1). Superposition of the α-carbons of HiPIP structures indicates that the *C. purpuratum* HiPIP is most closely related to the similarly sized *C. vinosum* HiPIP (0.41 Å rmsd), followed by *E. vacuolata* (rmsd = 0.58 Å), *E. halophila* (rmsd = 0.78 Å), and *Rc. tenuis* (rmsd = 1.18 Å).

The intracluster bonds in *C. purpuratum* HiPIP are similar to the oxidized form of *C. vinosum* HiPIP; they are relatively short and uniform as compared to those in the reduced form (*30*), suggesting the *C. purpuratum* HiPIP is oxidized in the crystals. The protein fold of *C. purpuratum* HiPIP in the vicinity of the iron−sulfur cluster is similar to that of other HiPIPs. The hydrogen bonding between the cysteinyl ligand sulfur atoms and amide nitrogen atoms is very similar to that tabulated for all of the HiPIP structures (see Table 8 in ref *16*). Likewise, in each of the structures, there is one potential hydrogen bond between a sulfur atom of the cluster (S1) and the amide nitrogen of Cys 75. This similarity in the cluster environment is at variance with the proposal that the hydrogen bonding from the immediate protein environment around the cluster is important in setting redox potential; the midpoint potential ranges between +120 and +390 mV for the HiPIPs for which structural data are available (Table 3).

In addition to the cysteines involved in bonding of the metal cluster, there are few highly conserved residues in HiPIP primary structures. The most conserved residues are found in three regions (*31*) and include Ala 14, Leu 17, Tyr 19, Asn 45, Phe 48, Gly 73, Trp 74, and Trp 78. With the exception of Asn 45, these residues are in close proximity to the metal cluster. As in *C. vinosum* HiPIP, there are five

Table 3: HiPIP Biochemical and Structural Data

organism	% identity with *C. purpuratum*	E_m (mV)[a]	space group	mol/ au	resol (Å)	PDB code
C. purpuratum		+390	$P2_12_12$	3	2.8	3HIP
C. vinosum	75.6	+346	$P2_12_12_1$	1	2.0	1HIP
Rc. tenuis (2761)	20.0	+310	$P2_1$	2	1.5	1ISU
E. halophila (iso-I)	28.4	+120	$P2_1$	2	2.5	2HIP
E. vacuolata (iso-II)	41.4	+172	$C222_1$	1	2.0	1HPI

[a] *C. purpuratum* HiPIP E_m from ref *21*. Others from the compilation of Heering et al. (*44*).

conserved aromatic amino acids in the vicinity of the *C. purpuratum* HiPIP metal cluster (Tyr 19, Phe 48, Phe 64, Trp 74, and Trp 78). Three of these (Tyr 19, Phe 48, and Phe 66) have recently been shown in *C. vinosum* to be essential in preventing degradation of the cluster, presumably by shielding it from solvent (*32*−*34*).

The Crystalline Dimers. The molecules in the *C. purpuratum* HiPIP crystals are tightly packed; the V_m is 1.9 Å^3/Da, corresponding to 34% solvent. Within the asymmetric unit, the three molecules appear to comprise one and one-half dimers. Two molecules form a dimer that relates the S4 apexes of the clusters by an approximate 2-fold axis of symmetry (Figure 1). The third molecule in the asymmetric unit is similarly oriented toward a second HiPIP molecule across the crystallographic 2-fold symmetry axis along *c*. In both the noncrystallographic and crystallographic dimer, the intercluster separation is similar to those observed in other crystalline HiPIP dimers (Table 4) and to the intercluster distances deduced from EPR data in *C. vinosum* HiPIP dimers (*13*). However, the two types of *C. purpuratum* HiPIP dimers are not completely superimposable (Table 4). Likewise, although each of the crystalline HiPIP dimers is similar in that the approximate 2-fold axis of symmetry allows close approach of the metal clusters and involves similar residues, the relative orientations of the two molecules within any dimer differs from that in the *C. purpuratum* noncrystallographic symmetry (NCS) or crystallographic symmetry (CS) dimers (Table 4). The *Rc. tenuis* dimer in which the two molecules are nearly related by 2-fold symmetry and the *E. vacuolata* crystallographic dimer were also compared to each other. They are related by a rotation angle of 43.2° and a negligible (0.1 Å) translation. Overall, the rotation necessary to relate the HiPIP dimers to one another indicates that the orientation of the two molecules across the dimerization interface is not conserved in the various HiPIPs. In this respect, it is of interest to note that the EPR data on the *C. vinosum* HiPIP suggest that it forms two different types of dimers, with intercluster distances of 13 and 16 Å (*13*).

In each case, the putative HiPIP dimerization interface is made up of three to four discontinuous segments of the protein chain (double underlined in Table 2), as is often observed in homodimers (*35*). With the exception of the *E. halophila* dimer, the short α-helical segment nearest the N-terminus of the protein (11−17 in *C. purpuratum*) forms one such segment. In a recent comparison of the primary structures of HiPIPs, Van Driessche et al. (*31*) mapped segments of the polypeptide chain, classified by conservation, onto the three-dimensional structure of *C. vinosum* HiPIP. In general, the most conserved regions of primary structure coincide with the putative dimerization interface. Despite the relatively low homology in primary structure (Table 3), the residues involved in dimerization are in similar positions with respect to the second, third, and fourth cysteinyl ligands (Table 2). Two of the most conserved residues in the primary structures of HiPIPs, Phe 48 and Leu 17, are at the center of the interface, flanking the buried S4 atom of the cluster (Figure 1). Likewise, the dimerization observed in *C. purpuratum* involves homologous residues predicted by Adman et al. (*19*) to be important in the *C. vinosum* dimer interface (Arg 33, Phe 48, and Gln 64). The dimerization interface also corresponds to the surface of *C. vinosum* HiPIP involved in the electron-transfer reactions with nonphysiological reactants (*36*).

The dimeric arrangement of the proteins in the crystal could be an artifact of crystallization, with the high salt concentration driving a nonspecific association of the flat, hydrophobic surfaces near the iron−sulfur clusters. Alternatively, one can argue that the predominantly nonpolar HiPIP dimer interface is typical of those found in oligomeric proteins. Oligomer interfaces favor nonpolar residues in contrast to crystal contacts which are typically characterized by numerous interactions between polar amino acids (*37*, *38*). Likewise the amount of surface area buried in each of the HiPIP dimers is within the range found in a tabulation of oligomer interfaces drawn from the Protein Data Bank (*35*).

Solution Studies of C. purpuratum HiPIP. Evidence for dimerization in solution is necessary to establish the functional relevance of the dimerization observed within the crystals. During purification of *C. purpuratum* HiPIP, it was noted that the protein migrates as an apparent dimer in size-exclusion chromatography. This behavior was consistent in several different mobile phases and column supports, suggesting that the elution is not affected by interaction with the column. A molecular mass for HiPIP purified for crystallization (at 8 mg/mL) of approximately 17 kDa was estimated by analytical size-exclusion chromatography using the TSK 3000 column (Figure 2). Iso-II HiPIP from *Rps. salinarum* (*20*) and *T. ferrooxidans* HiPIP (*10*) also behave as oligomers (tetramer and hexamer, respectively) in gel filtration.

C. purpuratum HiPIP appears to form SDS-stable HiPIP dimers (Figure 1 in ref *21*). The protein migrates as a dimer on the gel in the presence of β-mercaptoethanol; only boiling of the sample prior to electrophoresis results in migration consistent with a monomer. A similar observation of oligomeric migration in SDS−PAGE has been made for other HiPIPs; HiPIP isolated from *Thiocapsa pfennigii* migrates as a dimer with a minor trimeric form (*39*). This was attributed to the occurrence of disulfide interchange between the denatured molecules, despite treatment of the protein with β-mercaptoethanol. Similarly, β-mercaptoethanol does not abolish the *C. purpuratum* dimer observed in SDS−PAGE (*21*). *T. ferrooxidans* HiPIP is estimated by SDS−PAGE to be 63 kDa (*10*) or 24 kDa (*40*). Both the 63 and 24 kDa forms of *T. ferrooxidans* HiPIP on SDS−PAGE could be reduced to monomer only by boiling of the sample prior to electrophoresis. The 6 kDa monomer also forms oligomers of 12 and 26 kDa (*10*, *40*). EPR analysis of *T. ferrooxidans* HiPIP indicates a tetrameric organization in which the metal clusters interact cooperatively (*40*).

Table 4: High-Potential Iron−Sulfur Protein Dimers

organism	internal rot/tran[a]	differences between dimers[b]	SA buried (Å^2) per monomer	S4:S4 distance (Å)
C. purpuratum (NC)[c]	176.5°/−0.26 Å		394 (8.8%)	13.9
C. purpuratum (C)	(180°/0 Å)	65.3°/−0.37 Å	397 (8.9%)	13.1
Rc. tenuis (NC)	167.8°/−0.03 Å	153.1°/1.1 Å (NC) 91.5°/−3.6 Å (C)	354 (9.4%)	10.8
E. halophila (NC)	148.3°/2.15 Å	138.3°/6.6 Å (NC) 163.8°/16.5 Å (C)	409 (9.8%)	13.5
E. vacuolata (C)	(180°/0 Å)	167.2°/1.8 Å (NC) 172.2°/−2.5 Å (C)	277 (6.7%)	17.5

[a] The internal rotation and translation relating the two monomers within the dimer. [b] Other dimers are compared to the noncrystallographic and crystallographic *C. purpuratum* dimers. Individual monomers from the two different dimers are superimposed first. The values given describe the operation required to map the putative dimeric partners onto each other. [c] NC = dimer formed through noncrystallographic symmetry; C = dimer formed through crystallographic (2-fold) symmetry.

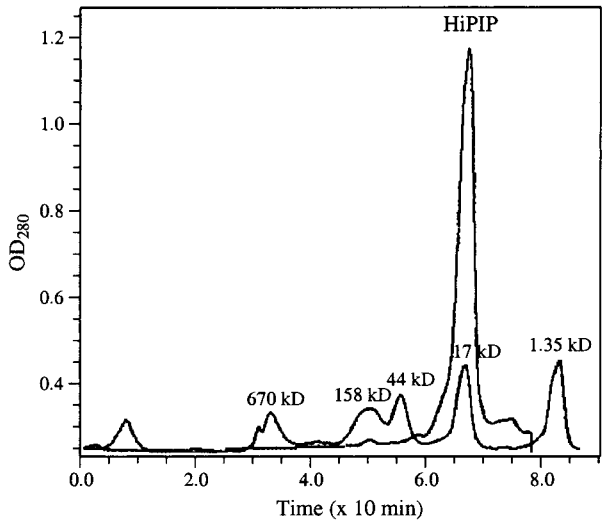

FIGURE 2: HPLC size-exclusion chromatography of HiPIP. The molecular mass standards (670, 158, 44, 17, and 1.35 kDa) are superimposed and labeled.

Light Scattering and Analytical Ultracentrifugation. The oligomeric state of *C. purpuratum* HiPIP was investigated by dynamic light scattering under several buffering conditions. Oxidized HiPIP in 50 mM Tris, pH 8.0, proved the most monodisperse: the average of 14 estimates yielded a molecular mass of 16.1 kDa. The size of reduced HiPIP was estimated to be 15.8 kDa (average of nine samplings) but the sample was polydisperse; the predicted range of particle sizes was 12−20 kDa. HiPIP in 50 mM sodium phosphate (presumably reduced) likewise appeared as a polydisperse solution of higher oligomeric states ranging 40−200 kDa (average of 12 samples). Although we anticipated a mixture of monomers and dimers at the protein concentration of 1−4 mg/mL, a species at 9 kDa was not detected under any conditions. This may indicate that the molecular mass estimates by this method are spurious.

Results of the analytical ultracentrifugation experiments on *C. purpuratum* HiPIP at 2.5 mg/mL indicated that the protein was monomeric. A gradual loss of material was apparent in 10 mM Tris, which was not observed after addition of 0.15 or 1.0 M sodium chloride. Aside from this putative sample depletion, no other ionic strength or pH effects were noted. The estimated molecular weight averaged from 10 runs (excluding in 10 mM Tris) was 9700 ± 400 Da. The observed sizes ranged from 9041 Da (in 10 mM sodium acetate, pH 5.0, and 1.0 M sodium chloride) to 12 216 Da (in 50 mM Tris, pH 8.0, and 100 mM glycine).

Due to the lack of unambiguous biochemical data for oligomerization, and the variation in the interdimer orientation of the different HiPIPs, the possibility that HiPIP dimerization plays a functional role remains speculative. Alternative explanations for the limited biochemical data supporting dimerization can be proposed. For example, the SDS−PAGE migration patterns observed may be an anomaly due to incomplete denaturation of the protein; boiling is necessary for full denaturation. HiPIP is at the low end of the size range that can be characterized accurately by the dynamic light scattering instrument so the molecular weight estimates by this technique may be unreliable. Likewise, the heterogeneity in the EPR spectra that has been interpreted to be a result of oligomerization can be ascribed to differences in electron distribution within the iron−sulfur cluster (*41*).

The equilibrium sedimentation studies are perhaps the freest from artifacts. They show that the protein is primarily monomeric under a variety of conditions for protein concentrations up to 2.5 mg/mL. Assuming that the dimer would have been detectable at a relative concentration of 10%, a lower bound for the dimer-to-monomer dissociation constant can be set at about 2 mM.

HiPIP may dimerize only under certain conditions or only at very high concentrations. The in vivo concentration of HiPIP relates to this point. On the basis of visual examination of Coomassie-stained denaturing gels, we estimate that HiPIP accounts for approximately 10−15% of the soluble protein in *C. purpuratum*. Since the periplasmic space makes up perhaps 30% of the cell volume, the concentration of HiPIP in the periplasm may be several tens of milligrams per milliliter, or several millimolar. Therefore, the modes of association occurring under crystallization conditions may be biologically relevant despite our inability to convincingly demonstrate such associations at lower concentrations.

Summary. A variety of experiments continue to give conflicting data regarding the possible dimerization of HiPIP. In the present study, the protein from *C. purpuratum* behaves as a dimer in size-exclusion chromatography as well as by light scattering, but as a monomer by ultracentrifugation. The crystal structure reveals two potential dimeric associations. An analysis of HiPIP crystal structures from this and other species supports a pronounced tendency for the protein to dimerize about a conserved, hydrophobic surface patch. However, the relative orientation of the monomers in different dimers varies so that the dimers are not superimposable. The lack of complete specificity in the self-

association weakens the argument for a biologically relevant dimer. To settle this issue, further functional studies will be required, perhaps using genetic or chemical methods to force or prevent the formation of long-lasting dimeric HiPIP variants.

ACKNOWLEDGMENT

We thank Cheryl Chan for her assistance in the purification of HiPIP and Dr. Martin Phillips of the UCLA-DOE Biochemistry Instrumentation Facility for making the analytical ultracentrifugation measurements. A preliminary report of these data appeared in ref *42*.

REFERENCES

1. Bruser, T., Truper, H. G., and Dahl, C. (1997) *Biochim. Biophys. Acta 1352*, 18−22.
2. Schoepp, B., Parot, P. Menin, L., Gaillard, J., Richaud, P., and Vermeglio, A. (1995) *Biochemistry 34*, 11736−11742.
3. Hochkoeppler, A., Ciurli, S., Venturoli, G., and Zannoni, D. (1995) *FEBS Lett. 357*, 70−74.
4. Hochkoeppler, A., Zannoni, D., Ciurli, S., Meyer, T. E., Cusanovich, M. A., and Tollin, G. (1996) *Proc. Natl. Acad. Sci. U.S.A.* 93, 6998−7002.
5. Menin, L., Schoepp, B., Parot, P., and Vermeglio, A. (1997) *Biochemistry 36*, 12183−12188.
6. Bruser, T., Truper, H. G., and Dahl, C. (1997) *IXth International Symposium on Photorophic Prokaryotes*, Abstr. 52A.
7. Hochkoeppler, A., Kofod, P., and Zannoni, D. (1995) *FEBS Lett. 375*, 197−200.
8. Fukomori, Y., and Yamanaka, T. (1979) *Curr. Microbiol 3*, 117−120.
9. Tedro, S. M., Meyer, T. E., and Kamen, M. D. (1977) *J. Biol. Chem. 252*, 7826−7833.
10. Kusano, T., Takeshima, T., Sugawara, K., Inoue, C., Shiratori, T., Yano, T., Fukomori, Y., and Yamanaka, T. (1992) *J. Biol. Chem.267*, 11242−11247.
11. Roualt, T., and Klausner, R. D. (1996) *Trends Biochem. Sci. 21*, 174−177.
12. Bertini, I., Gaudemer, A., Luchinat, C., and Piccioli, M. (1993) *Biochemistry 32*, 12887−12893.
13. Dunham, W. R., Hagen, W. R., Fee, J. A., Sands, R. H., Dunbar, J. B., and Humblet, C. (1991) *Biochim. Biophys. Acta 1079*, 253−262.
14. Carter, C. W., Kraut, J., Freer, S. T., and Alden, R. A. (1974) *J. Biol. Chem. 249*, 6339−6346.
15. Breiter, D. R., Meyer, T. E., Rayment, I., and Holden, H. M. (1991) *J. Biol. Chem. 266*, 18660−18667.
16. Rayment, I., Wesenberg, G., Meyer, T. E., Cusanovich, M. A., and Holden, H. M. (1992) *J. Mol. Biol. 228*, 672−686.
17. Benning, M. W., Meyer, T. E., Rayment, I., and Holden, H. M. (1994) *Biochemistry 33*, 2476−2483.
18. Schubert, W.-D., Klukas, O., Krauss, N., Saenger, W., Fromme, P., and Witt, H. T. (1997) *J. Mol. Biol. 272*, 741−769.
19. Adman, E. T., Mather, M. W., and Fee, J. A. (1993) *Biochim. Biophys. Acta 1142*, 93−98.
20. Meyer, T. E., Fitch, J., Bartsch, R. G., Tollin, D., and Cusanovich, M. A. (1990) *Biochim. Biophys. Acta 1017*, 118−124.
21. Kerfeld, C. A., Chan, C., Hirasawa, M., Kleiss-SanFrancisco, S., Yeates, T. O., and Knaff, D. B. (1996) *Biochmistry 35*, 7812−7818.
22. Otwinowski, Z. (1993) in *Data Collection and Processing* (Sawyer, L., Isaacs, N., and Bailey, S., Eds.) pp 56−62, Daresbury Laboratory, Warrington.
23. Navaza, J. (1994) *Acta Crystallogr., Sect. A 50*, 157−163.
24. Brünger, A. T. (1992) XPLOR Manual, version 3.1, Yale University Press, New Haven, CT.
25. Collaborative Computational Project, Number 4 (1994) *Acta Crystallogr., Sect. D 50*, 760−763.
26. Jones, T. A. (1978) *J. Appl. Crystallogr. 11*, 268−272.
27. Engh, R. A., and Huber, R. (1991) *Acta Crystallogr., Sect. A 47*, 392−400.
28. Satow, Y., Cohen, G. H., Padlan, E. A., and Davies, R. (1986) *J. Mol. Biol. 190*, 593−604.
29. Handschumacher, M. D., and Richards, F. M. (1994) *Acta Crystallogr., Sect. D 50*, 760−763.
30. Carter, C. W., Kraut, J., Freer, S. T., Alden, R. A., Sieker, L. C., Adman, E., and Jensen, L. H. (1974b). *Proc. Natl. Acad. Sci. U.S.A. 69*, 3526−3529.
31. Van Driessche, Ciurli, S., Hochkoeppler, A., and VanBeeumen, J. (1997) *Eur J. Biochem. 244*, 371−377.
32. Agarwal, A., Li, D., and Cowan, J. A. (1995) *Proc. Natl. Acad. Sci U.S.A. 92*, 9440−9444.
33. Soriano, A., and Cowan, J. A. (1996) *Inorg. Chim. Acta 251*, 285−290.
34. Bian, S., Hemann, C. F., Hille, R., and Cowan, J. A. (1996) *Biochemistry 35*, 14544−14552.
35. Jones, S., and Thornton, J. M. (1996) *Proc. Natl. Acad. Sci. U.S.A. 93*, 13−20.
36. Mizrahi, I. A., Meyer, T. E., and Cusnaovich, M. A. (1980) *Biochemistry 19*, 4727−4733.
37. Janin, J., Miller, S., and Chothia, C. (1988) *J. Mol. Biol. 204*, 155−164.
38. Dasgupta, S., Iyer, G. H., Bryant, S. H., Lawrence, C. E., and Bell, J. A. (1997) *Proteins: Struct., Funct., Genet. 28*, 494−514.
39. Meyer, T. E., Kennel, S. J., Tedro, S. M., and Kamen, M. D. (1973) *Biochim. Biophys. Acta 292*, 634−643.
40. Cavazza, C., Guigliarelli, B, Bertrand, P., and Bruschi, M. (1995) *FEMS Micro. Lett. 130*, 193−199.
41. Banci, L., Bertini, I, Ciurli, S., Ferreti, S., Luchinat, L., and Piccioli, M. (1993) *Biochemistry 32*, 9387−9397.
42. Kerfeld, C. A., Chan, C., and Yeates, T. O. (1995) in *Photosynthesis: from Light to Biosphere*, Proceedings of the Xth International Photosynthesis Congress (Mathis, P., Ed.) pp 757−760, Kluwer Academic Publishers, Boston.
43. Kraulis, P. J. (1991) *J. Appl. Crystallogr. 24*, 946−950.
44. Heering, H. A., Bulsink, Y. B. M., Hagen, W. R., and Meyer, T. E. (1995) *Biochemistry 34*, 14675−14686.

BI9810252